Corrected 28 July 2015; see full text.

no protection against SIVmac251 challenges (*3*), which reflects the ability of DNA/Ad5 vaccines to block only neutralization-sensitive virus clones (*35*). Alphavirus vector priming and Env protein boosting afforded partial protection against the neutralization-sensitive virus SHIV-SF162P4 but was not evaluated against neutralization-resistant viruses (*36*). Rhesus cytomegalovirus (CMV) vectors failed to block acquisition of infection but afforded post-infection virologic control and eventual viral clearance in about half of the animals after SIVmac239 challenges (*28*, *37*).

The protective efficacy of Ad/Env vaccines against acquisition of neutralization-resistant virus challenges in rhesus monkeys in the present study has important implications for HIV-1 vaccine development and suggests the potential of Env protein boosting after Ad vector priming. Nevertheless, important differences exist between SIV/SHIV infection in rhesus monkeys and HIV-1 infection in humans. Clinical efficacy studies are therefore required to determine the protective efficacy of these HIV-1 vaccine candidates in humans.

REFERENCES AND NOTES

1. A. S. Fauci, H. D. Marston, *N. Engl. J. Med.* **370**, 495–498 (2014).
2. D. H. Barouch, *N. Engl. J. Med.* **369**, 2073–2076 (2013).
3. N. L. Letvin *et al.*, *Sci. Transl. Med.* **3**, 81ra36 (2011).
4. S. M. Hammer *et al.*, *N. Engl. J. Med.* **369**, 2083–2092 (2013).
5. D. H. Barouch *et al.*, *Nature* **482**, 89–93 (2012).
6. D. H. Barouch *et al.*, *Cell* **155**, 531–539 (2013).
7. P. Abbink *et al.*, *J. Virol.* **81**, 4654–4663 (2007).
8. B. Chen *et al.*, *J. Biol. Chem.* **275**, 34946–34953 (2000).
9. R. Vogels *et al.*, *J. Virol.* **77**, 8263–8271 (2003).
10. J. P. Nkolola *et al.*, *J. Virol.* **84**, 3270–3279 (2010).
11. D. Montefiori, *Curr. Protoc. Immunol.* **Chap. 12** (Unit 12.11), 1–15 (2005).
12. A. W. Chung, G. Alter, *Future Virol* **9**, 397–414 (2014).
13. M. E. Ackerman, G. Alter, *Curr. HIV Res.* **11**, 365–377 (2013).
14. M. E. Ackerman *et al.*, *J. Immunol. Methods* **366**, 8–19 (2011).
15. V. R. Gómez-Román *et al.*, *J. Immunol. Methods* **308**, 53–67 (2006).
16. A. W. Chung *et al.*, *Sci. Transl. Med.* **6**, 228ra38 (2014).
17. E. P. Brown *et al.*, *J. Immunol. Methods* **386**, 117–123 (2012).
18. A. W. Boesch *et al.*, *MAbs* **6**, 915–927 (2014).
19. K. S. Lau *et al.*, *Sci. Signal.* **4**, ra16 (2011).
20. L. J. Picker *et al.*, *J. Clin. Invest.* **116**, 1514–1524 (2006).
21. H. Li *et al.*, *J. Virol.* **85**, 11007–11015 (2011).
22. J. Liu *et al.*, *Nature* **457**, 87–91 (2009).
23. J. Liu *et al.*, *J. Virol.* **84**, 10406–10412 (2010).
24. S. A. Handley *et al.*, *Cell* **151**, 253–266 (2012).
25. E. Aronesty, in code.google.com/p/ea-utils. (ea-utils, Durham, NC, 2011).
26. L. Fu, B. Niu, Z. Zhu, S. Wu, W. Li, *Bioinformatics* **28**, 3150–3152 (2012).
27. D. H. Huson, S. Mitra, H.-J. Ruscheweyh, N. Weber, S. C. Schuster, *Genome Res.* **21**, 1552–1560 (2011).
28. S. G. Hansen *et al.*, *Nature* **502**, 100–104 (2013).
29. D. H. Barouch *et al.*, *Nat. Med.* **16**, 319–323 (2010).
30. J. M. Kovacs *et al.*, *Proc. Natl. Acad. Sci. U.S.A.* **109**, 12111–12116 (2012).
31. A. Masch, J. Zerweck, U. Reimer, H. Wenschuh, M. Schutkowski, *Methods Mol. Biol.* **669**, 161–172 (2010).
32. K. E. Stephenson *et al.*, *J. Immunol. Methods* **416**, 105–123 (2015).
33. S. Rerks-Ngarm *et al.*, *N. Engl. J. Med.* **361**, 2209–2220 (2009).
34. B. F. Haynes *et al.*, *N. Engl. J. Med.* **366**, 1275–1286 (2012).
35. M. Roederer *et al.*, *Nature* **505**, 502–508 (2014).
36. S. W. Barnett *et al.*, *J. Virol.* **84**, 5975–5985 (2010).
37. S. G. Hansen *et al.*, *Nature* **473**, 523–527 (2011).

ACKNOWLEDGMENTS

We thank M. Pensiero, M. Marovich, M. Beck, J. Kramer, S. Westmoreland, P. Johnson, W. Wagner, J. Yalley, C. Gittens, C. Cosgrove, M. Kumar, J. Schmitz, H. Peng, J. Hendriks, D. van Manen, W. Bosche, V. Cyril, Y. Li, F. Stephens, R. Hamel, K. Kelly, and L. Dunne for generous advice, assistance, and reagents. The SIVmac239 peptides were obtained from the NIH AIDS Research and Reference Reagent Program. The data presented in this paper are tabulated in the main paper and in the supplementary materials. The authors declare no competing financial interests. D.H.B. is a named co-inventor on vector, antigen, and protein patents (PCT/EP2007/052463, PCT/US2009/060494, PCT/US2009/064999). Correspondence and requests for materials should be addressed to D.H.B. (dbarouch@bidmc.harvard.edu). Vectors, antigens, proteins, adjuvants, and viruses are subject to Material Transfer Agreements. We acknowledge support from the NIH (AI060354, AI078526, AI080289, AI084794, AI095985, AI096040, AI102660, AI102691, OD011170, and HHSN261200800001E), the Bill and Melinda Gates Foundation (OPP1032817), and the Ragon Institute of MGH, MIT, and Harvard.

SUPPLEMENTARY MATERIALS

www.sciencemag.org/content/349/6245/320/suppl/DC1
Materials and Methods
Figs. S1 to S15
References

20 April 2015; accepted 17 June 2015
Published online 2 July 2015;
10.1126/science.aab3886

CIRCADIAN RHYTHMS

A protein fold switch joins the circadian oscillator to clock output in cyanobacteria

Yong-Gang Chang,[1] Susan E. Cohen,[2] Connie Phong,[3] William K. Myers,[4] Yong-Ick Kim,[2] Roger Tseng,[1,5] Jenny Lin,[3] Li Zhang,[1] Joseph S. Boyd,[2] Yvonne Lee,[6] Shannon Kang,[6] David Lee,[7] Sheng Li,[7] R. David Britt,[4] Michael J. Rust,[3] Susan S. Golden,[2,6] Andy LiWang[1,2,5,8,9]*

Organisms are adapted to the relentless cycles of day and night, because they evolved timekeeping systems called circadian clocks, which regulate biological activities with ~24-hour rhythms. The clock of cyanobacteria is driven by a three-protein oscillator composed of KaiA, KaiB, and KaiC, which together generate a circadian rhythm of KaiC phosphorylation. We show that KaiB flips between two distinct three-dimensional folds, and its rare transition to an active state provides a time delay that is required to match the timing of the oscillator to that of Earth's rotation. Once KaiB switches folds, it binds phosphorylated KaiC and captures KaiA, which initiates a phase transition of the circadian cycle, and it regulates components of the clock-output pathway, which provides the link that joins the timekeeping and signaling functions of the oscillator.

Endogenous circadian (~24-hour) rhythms are found in diverse organisms, arising as an adaptation to Earth's persistent cycles of day and night (*1*). To uncover the molecular mechanism of a circadian clock, we chose the cyanobacterial system because its oscillator can be reconstituted in vitro (*2*). The oscillator is composed of only three proteins KaiA, KaiB, and KaiC (*3*), which together generate a circadian rhythm of KaiC phosphorylation at residues serine 431 (S431) and threonine 432 (T432) in the CII domain (*4*, *5*). KaiA promotes KaiC (auto)phosphorylation during the subjective day (*4*, *6*), whereas KaiB provides negative feedback to inhibit KaiA (*7*, *8*) and promotes KaiC (auto)dephosphorylation during the subjective night. KaiB is also involved in regulating two antagonistic clock-output proteins—SasA (*9*) and CikA (*10*), which reciprocally control the master regulator of transcription, RpaA (*11*).

To determine the structure of KaiB in its KaiC-bound state, we used a monomeric variant of the KaiB-binding domain of KaiC, CI*, and a dimeric KaiB variant (*12*), KaiB*, with enhanced KaiC binding. Dimeric forms of free KaiB retain the same tertiary structure in crystals as tetrameric forms (*13*). Free KaiB has been shown by x-ray crystallography (*14*) to adopt a fold found in no other protein (*15*), despite clear sequence similarity with the thioredoxin-like fold at the N terminus of SasA, N-SasA (*9*). For structural studies, we used proteins from *Thermosynechococcus elongatus* (denoted by ^{te}), because they are more stable than those from *Synechococcus elongatus* (*16*). For functional studies, we used proteins from *S. elongatus* (denoted by ^{se}),

[1]School of Natural Sciences, University of California, Merced, CA 95343, USA. [2]Center for Circadian Biology, University of California, San Diego, La Jolla, CA 92093, USA. [3]Department of Molecular Genetics and Cell Biology, University of Chicago, Chicago, IL 60637, USA. [4]Department of Chemistry, University of California, Davis, CA 95616, USA. [5]Quantitative and Systems Biology, University of California, Merced, CA 95343, USA. [6]Division of Biological Sciences, University of California, San Diego, La Jolla, CA 92093, USA. [7]Department of Medicine, University of California, San Diego, La Jolla, CA 92093, USA. [8]Chemistry and Chemical Biology, University of California, Merced, CA 95343, USA. [9]Health Sciences Research Institute, University of California, Merced, CA 95343, USA.
***Corresponding author. E-mail: aliwang@ucmerced.edu**

Corrected 28 July 2015; see full text.

the standard model for investigating in vivo circadian rhythms (*17*). Analytical ultracentrifugation experiments indicated that KaiB^{te}* binds to CI^{te}* as a monomer with a stoichiometric ratio of 1:1 (fig. S1A). Secondary chemical shifts of backbone resonances (*18*) of KaiB^{te}* in complex with CI^{te}* (fig. S1) revealed a thioredoxin-like secondary structure (βαβαββα) (*19*), rather than the secondary structure of free KaiB (βαββααβ) found in protein crystals (Fig. 1A). Hereafter, we refer to the βαββααβ form of KaiB as the ground state (gsKaiB), and the βαβαββα state as fold-switched KaiB (fsKaiB). Fewer than 10 proteins are known to switch reversibly between distinct folds under native conditions, and they are collectively known as metamorphic proteins (*20*). KaiB is the only metamorphic protein known to function in biological clocks.

Along a β strand, side chains typically alternate ↑↓↑↓.... In the β4 strand of gsKaiB, the side chain pattern is ↑↓–↑, where the dash is G89; in fsKaiB, G89 lies in the α3 helix. We reasoned that a G89A substitution would destabilize β4 in gsKaiB but not α3 in fsKaiB (Fig. 1B). A D91R substitution should also destabilize gsKaiB by disrupting a putative salt bridge with K58. Nuclear magnetic resonance secondary chemical-shift analysis revealed that, unlike KaiB^{te}*, the two single-point mutants had populations of both gsKaiB and fsKaiB states, but only the fsKaiB state was detected in the double-mutant (figs. S2 to S6). A structural model of G89A,D91R-KaiB^{te}* determined by CS-Rosetta (*21*), using chemical shifts and backbone amide $^{1}H^{N}$–$^{1}H^{N}$ nuclear Overhauser effects as restraints, confirmed that G89A,D91R-KaiB^{te}* adopted a thioredoxin-like fold (fig. S7), similar to that of N-SasA (*22*).

The corresponding KaiB variants in *S. elongatus*, G88A-KaiB^{se}, D90R-KaiB^{se}, and G88A,D90R-KaiB^{se} also promoted the fsKaiB state relative to wild-type (WT) KaiB^{se} (figs. S8 and S9). G88A, D90R-KaiB^{se} formed a complex with CI^{se}*, with near-complete binding within 5 min (fig. S10). In contrast, WT KaiB^{se} bound CI^{se}* marginally, even after 24 hours (fig. S11). In vitro oscillation assays showed that the KaiB^{se} variants disrupted KaiC^{se} phosphorylation rhythms (Fig. 2A and fig. S12). Amounts of KaiC^{se} phosphorylation were larger in the presence of D90R-KaiB^{se} or G88A, D90R-KaiB^{se} than they were with G88A-KaiB^{se}. G88A-KaiB^{se} formed a complex with KaiA^{se} (Fig. 2B), whereas the two KaiB^{se} mutants containing D90R did not (fig. S13), which indicated that although the D90R mutation promotes the fsKaiB state, it also disrupts binding. Larger amounts of unsequestered KaiA would be expected to lead to larger amounts of KaiC phosphorylation, which would account for the observed differences in the KaiC phosphorylation profiles when the D90R mutants were used. In vivo bioluminescence rhythms from cyanobacterial luciferase reporter strains harboring *kaiB*^{se} variants (Fig. 2C) were also disrupted, with phenotypes that agreed with the in vitro phosphorylation patterns (Fig. 2A). A chromosomal copy of *kaiB*$^{+}$ in addition to the mutant *kaiB* variants did not restore bioluminescence rhythms in vivo, which indicated a dominant-negative effect of the fold-switch mutations (Fig. 2D and fig. S14). KaiB fold switch–stabilizing mutants are less abundant in vivo than WT KaiB (fig. S15), so at equilibrium in vivo fsKaiB is probably rare.

Although KaiB^{se} variants disrupted rhythms in vitro and in vivo, each of them restored the cell-length phenotype in *kaiB*$^{-}$ strains (Fig. 2, E and F) in which the SasA-RpaA output pathway was hyperstimulated and cell division was inhibited (*23*). These functional variants indicate that fsKaiB regulates the clock-output enzymes SasA (*9*) and CikA (*10*, *23*). SasA is activated when it binds KaiC (*24*), and SasA and KaiB compete for the CI domain of KaiC (*25*). Preincubation with the D90R-KaiB^{se} and G88A,D90R-KaiB^{se} variants inhibited the ability of S431E-KaiC^{se} (a KaiC variant that mimics phosphorylation at the S431 residue) to trigger output signaling through SasA^{se} (Fig. 2G and fig. S16). Also, mixtures of KaiB and KaiC activate the phosphatase activity of CikA that dephosphorylates RpaA (*26*). Relative to WT KaiB^{se}, fsKaiB^{se} variants enhanced CikA^{se} phosphatase activity by about threefold in vitro (Fig. 2H and fig. S17) and suppressed RpaA^{se} phosphorylation in vivo (fig. S18). We propose that fsKaiB forms a complex with KaiC that both activates signaling through CikA and inhibits signaling through SasA by outcompeting SasA for binding to KaiC. It is likely that fsKaiB interacts with the CikA pseudo-receiver domain (PsR-CikA), because adding PsR-CikA to the in vitro oscillator shortened the period and reduced the amplitude (Fig. 2I and fig. S19). Overexpression of just the PsR-CikA domain in cyanobacteria similarly shortened the period of bioluminescence rhythms (*27*). Interaction with PsR-CikA was detected for G88A,D90R-KaiB^{se}, but not KaiB^{se} (fig. S20). Addition of the PsR domain of KaiA did not affect phosphorylation rhythms (Fig. 2J), even though it has the same tertiary structure as PsR-CikA (*6*, *28*).

fsKaiB/gsKaiB equilibrium constants, $K = k_{B+}/k_{B-}$, were estimated by fitting the kinetics of binding of KaiB^{te} variants to CI^{te}* (fig. S21). Equilibrium constants were larger for G89A-KaiB^{te} (K = 0.13 ± 0.02), D91R-KaiB^{te} (1.2 ± 0.1), and G89A,D91R-KaiB^{te} (6.7 ± 0.4), relative to KaiB^{te} (0.08 ± 0.01). For KaiB^{te} variants binding S431E-KaiC^{te}, a distinct fast-binding phase was followed by slow binding (Fig. 3A). These multiphase binding kinetics were reproduced in a gsKaiB ⇔ fsKaiB fold-switching model (Fig. 3B), in which KaiB was initially at equilibrium between the two folds. The pool of fsKaiB bound

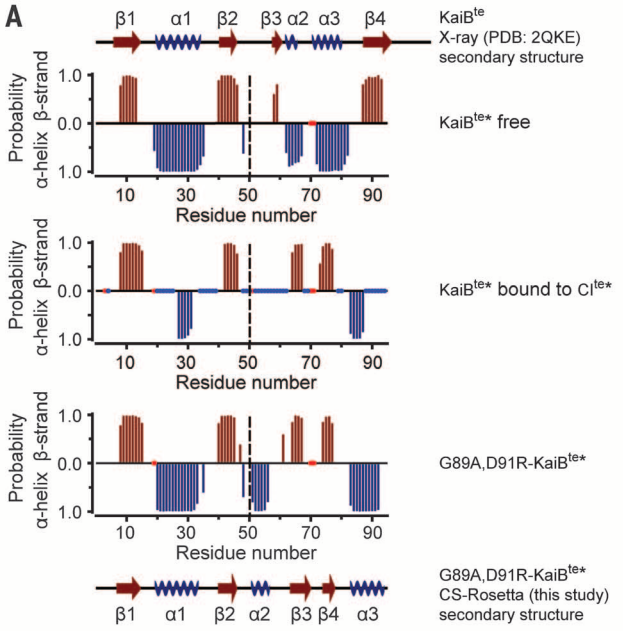

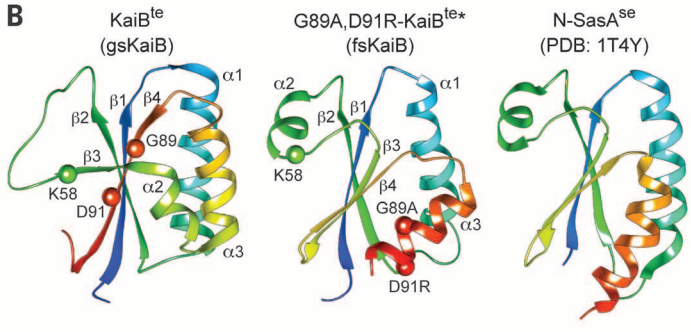

Fig. 1. KaiB switches its fold to bind KaiC. (**A**) Plots of chemical shift–based secondary structures of KaiB^{te}*, KaiB^{te}* + CI^{te}*, and G89A,D91R-KaiB^{te}* determined by TALOS+ (*18*). Unassigned proline and nonproline residues are indicated by small red and blue dots along the horizontal axis at y = 0. The secondary structures of KaiB^{te} and G89A,D91R-KaiB^{te}* are shown for comparison. KaiB^{te}* residues Q52 to E56 in KaiB^{te}* bound to CI^{te}* were not assignable, probably owing to exchange broadening. Vertical dashed lines are visual guides separating the N-terminal and C-terminal halves of KaiB. (**B**) Structural comparisons of KaiB^{te}, G89A,D91R-KaiB^{te}*, and N-SasA^{se}. Residues K58, G89, and D91 are highlighted for their roles in fold switching.

Corrected 28 July 2015; see full text.

rapidly upon adding S431E-KaiC (Fig. 3C), followed by a slow gsKaiB → fsKaiB population shift. As shown by our computational model (Fig. 3B and fig. S22), the slow formation of the KaiB-KaiC complex contributes to the delay that allows a population of KaiC proteins to become highly phosphorylated under continued stimulation by KaiA. Increasing the rate of KaiB-KaiC binding in our model causes the in silico phosphorylation rhythm to fail (Fig. 3D), similar to that observed in vitro. Comparing the kinetics of binding to CI (fig. S21) and full-length KaiC (Fig. 3A) by KaiB mutants shows that full-length KaiC contributes to the slow phase as well, and this is likely due to the CI adenosine triphosphatase (*29*) exposing the KaiB-binding site upon its activation by CI-CII ring stacking (*12*).

N-SasA, which also adopts a thioredoxin-like fold (*22*), competes with KaiB for binding KaiC (*25*) (fig. S23). Intermolecular distances for the complexes CI^{te}*–N-$SasA^{te}$ and CI^{te}*–G89A,D91R-$KaiB^{te}$* (figs. S24 and S25) were measured by using the pulsed electron paramagnetic resonance method of double electron-electron resonance (DEER), in combination with mutagenesis studies (figs. S26 to S29). The higher-quality DEER data for the CI^{te}*–N-$SasA^{te}$ complex allowed structural modeling (Fig. 4A and figs. S30 and S31). In this model, the α2 helix of N-SasA binds to the B-loop region of the CI domain (residues A109 to D123), with additional interactions involving the CI α-helix that follows. Hydrogen-deuterium exchange mass spectrometry (HDX-MS) data on both complexes (Fig. 4, A and B, and figs. S32 to S35) also suggest that this region of KaiC is a common binding site for KaiB and SasA. This model is consistent with a report that truncation of the B loop abolished binding (*25*). B-loop truncation also restored the cell-length phenotype of a strain that lacked *kaiB* (fig. S36). Furthermore, a F121A mutation in the B loop of full-length KaiC (F121A-S431E-$KaiC^{se}$) abolished KaiC binding

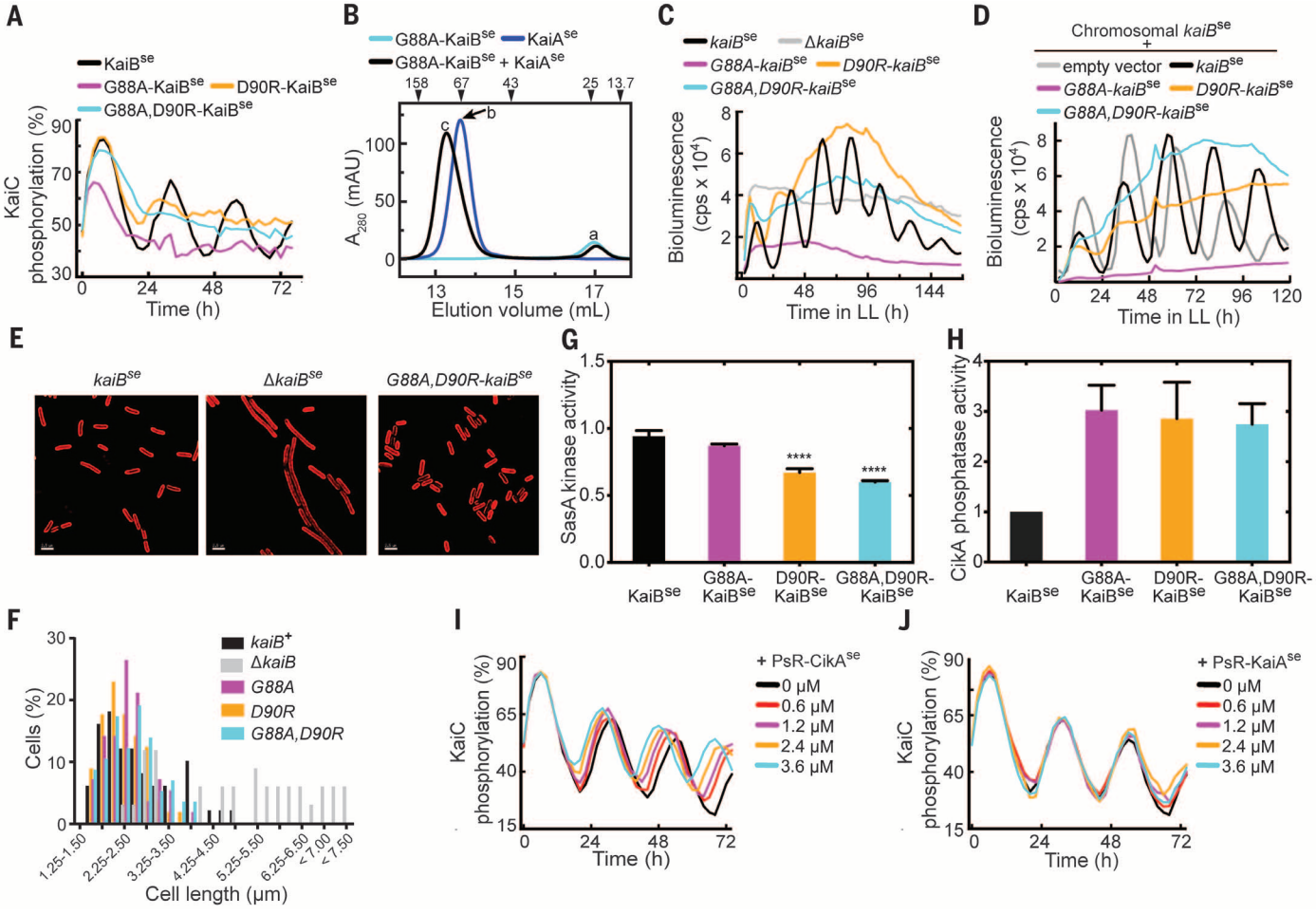

Fig. 2. KaiB fold switching regulates oscillator function and clock output. (**A**) In vitro KaiC phosphorylation assays using $KaiC^{se}$, $KaiA^{se}$, and $KaiB^{se}$, G88A-$KaiB^{se}$, D90R-$KaiB^{se}$, or G88A,D90R-$KaiB^{se}$. (**B**) Gel-filtration profiles of G88A-$KaiB^{se}$, $KaiA^{se}$, and G88A-$KaiB^{se}$ + $KaiA^{se}$. Peaks (a) to (c) were analyzed by SDS–polyacrylamide gel electrophoresis (fig. S13). (**C**) Bioluminescence from strains that carry a P_{kaiB} *luc* reporter for circadian rhythmicity. Cells harbored *kaiB*^{se}, *G88A-kaiB*^{se}, *D90R-kaiB*^{se}, or *G88A,D90R-kaiB*^{se}, or cells with *kaiB*^{se} deletion. Time in LL, time under low-light conditions. (**D**) Bioluminescence from strains that carry a P_{kaiB} *luc* reporter expressing *kaiB*^{se}, *G88A-kaiB*^{se}, *D90R-kaiB*^{se}, *G88A,D90R-kaiB*^{se}, or empty vector, in addition to chromosomal *kaiB*^{se}. (**E**) Representative micrographs of cells expressing *kaiB*^{se}, lacking *kaiB*^{se}, or harboring *G88A, D90R-kaiB*^{se}. Cellular autofluorescence in red. Scale bars, 2.5 μm. (**F**) Histograms showing cell-length distributions of strains expressing *kaiB*^{se}, *ΔkaiB*^{se}, *G88A-kaiB*^{se}, *D90R-kaiB*^{se}, or *G88A,D90R-kaiB*^{se} as the only copy of *kaiB*. (**G**) $SasA^{se}$ kinase activities in the presence of S431E-$KaiC^{se}$ and $KaiB^{se}$, G88A-$KaiB^{se}$, D90R-$KaiB^{se}$, or G88A,D90R-$KaiB^{se}$. The mixtures were incubated for 2 hours before $SasA^{se}$, $RpaA^{se}$ and [γ–^{32}P]ATP (^{32}P-labeled adenosine triphosphate) were added. Relative kinase activities compare the mean steady-state amount of ^{32}P-labeled $RpaA^{se}$ to that of a reaction without KaiB (n = 4, error bars denote SEM). One-way analysis of variance (ANOVA) gives $P < 0.001$, and **** denotes Bonferroni-corrected values ($P < 0.001$) for pairwise comparisons against kinase activity with $KaiB^{se}$ (α = 0.05). (**H**) CikA phosphatase activity toward phosphorylated RpaA in the presence of $KaiC^{se}$ and $KaiB^{se}$, G88A-$KaiB^{se}$, D90R-$KaiB^{se}$, or G88A,D90R-$KaiB^{se}$ (n = 4–5, error bars denote SEM). $KaiC^{se}$ alone or $KaiB^{se}$ alone did not activate CikA phosphatase activity (fig. S17). (**I**) In vitro $KaiC^{se}$ phosphorylation assays as a function of concentration of PsR-$CikA^{se}$. (**J**) Same as (I) except for using PsR-$KaiA^{se}$ instead of PsR-$CikA^{se}$. The black curves in (I) and (J) are identical.

Corrected 28 July 2015; see full text.

to full-length SasA^{se}, KaiB^{se}, and G88A,D90R-KaiB^{se} (figs. S37 to S40). HDX-MS data (Fig. 4, A and B) indicated that N-SasA and KaiB induce long-range perturbations in isolated CI domains that, in the context of full-length KaiC, may affect intersubunit interactions. Another HDX-MS–derived model (*30*) indicated that KaiB most likely binds to CII, on the basis of a calculation minimizing the docking energy between KaiC and gsKaiB, not fsKaiB.

Naturally occurring variations at residue positions 58, 89, and 91 of KaiB (fig. S41A) suggest that the ancestral KaiB protein had the fsKaiB thioredoxin-like fold, and the gsKaiB fold evolved later with the circadian clock. In support of

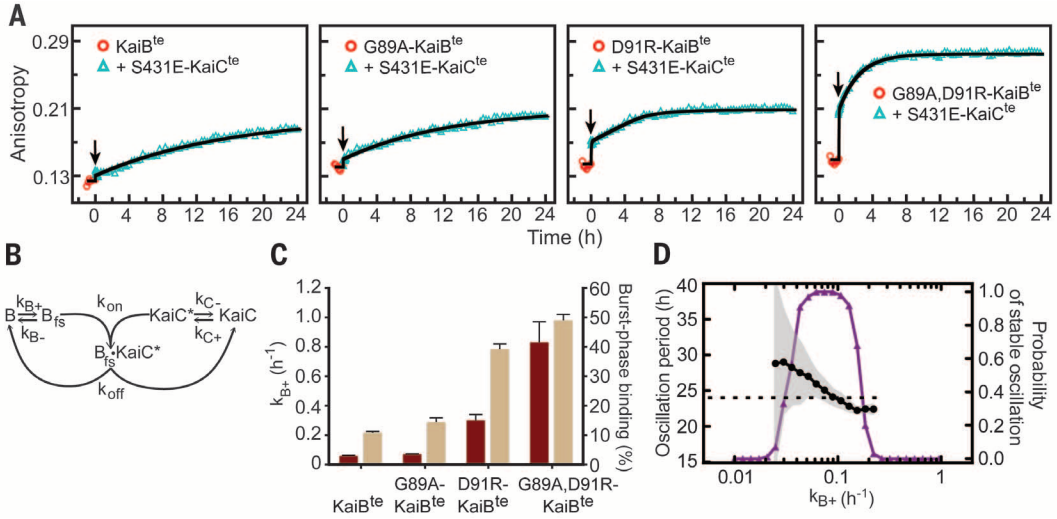

Fig. 3. KaiB fold-switching regulates slow formation of the KaiB-KaiC complex. (**A**) Fluorescence anisotropies of 6-iodoacetamidofluorescein (6-IAF)–labeled KaiB^{te}, G89A-KaiB^{te}, D91R-KaiB^{te}, and G89A,D91R-KaiB^{te} in the presence of S431E-KaiC^{te}. KaiB samples were incubated for 1 hour (circles) before addition (arrow) of S431E-KaiC^{te}. A54C mutation was introduced to all KaiB for fluorescence labeling. (**B**) Scheme for modeling. (**C**) Forward fold-switching rate constants, k_{B+} (maroon), and burst-phase binding to S431E-KaiC^{te} (tan). Burst-phase binding—defined as the percentage of KaiB^{te}-S431E-KaiC^{te} complexes formed at t = 0.1 hours in the model relative to steady-state binding at t = 24 hours—were derived from fitting data after adding S431E-KaiC^{te} in (A) to the model shown in (B). Burst-phase error bars show the standard deviation from model calculations by bootstrap resampling the raw data (n = 20). k_{B+} values used in these fits were predetermined from analysis of the kinetics of binding of KaiB^{te} variants to the isolated CI^{te}* domain (fig. S21), a condition where we assumed the rate-limiting step in complex formation is due only to KaiB fold switching. Error bars for k_{B+} were estimated by bootstrap resampling the original data set 500 times. (**D**) Mathematical modeling of KaiC phosphorylation period (black) and probability of stable oscillation (purple), as a function of the forward fold-switching rate constant, k_B+. Each black point represents the mean period from 100 simulations at fixed k_B+, while randomly varying all other parameters (Gaussian with 10% standard deviation). The shaded region represents standard deviations of the periods for those parameter sets that produced stable oscillations. Oscillations became unstable outside of the plotted range. The purple plot is the fraction of simulations that produced stable oscillations at each k_B+ value. The dashed line runs parallel to the x axis and intersects the y axis at 24 hours.

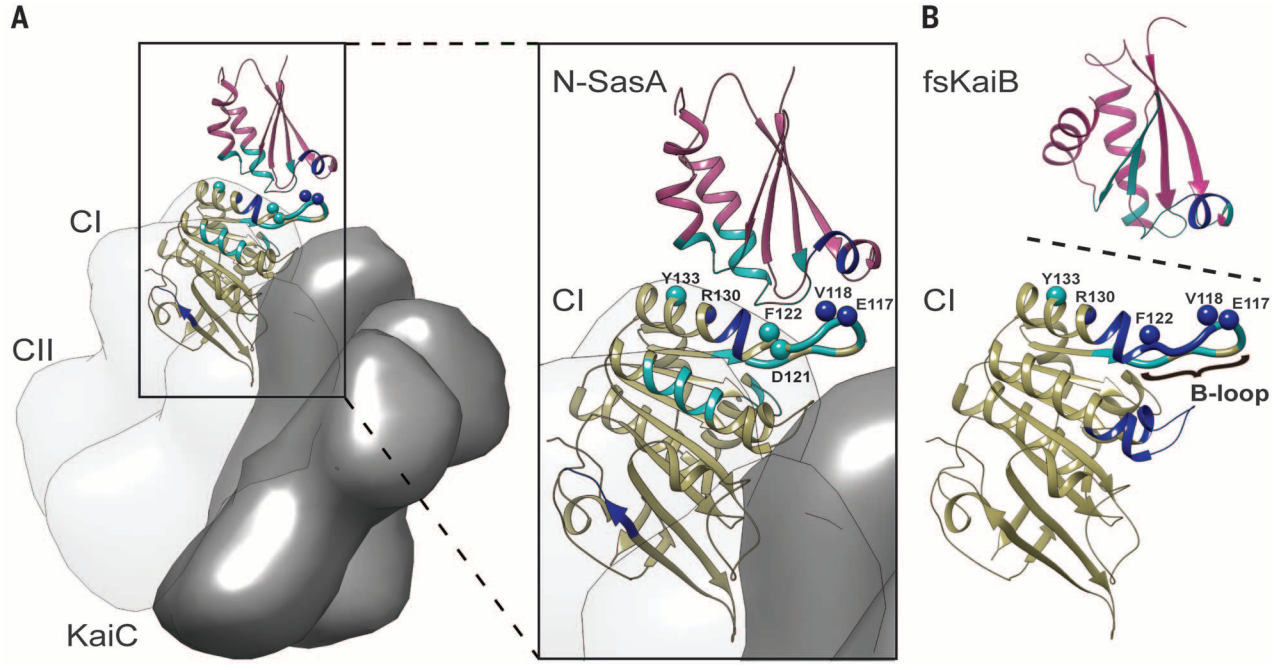

Fig. 4. KaiB and SasA bind to similar sites on CI. (**A**) An electron paramagnetic resonance–restrained model of the CI^{te}*–N-SasA^{te} complex. The HADDOCK (*32*) model of the complex with the best score is superimposed on the crystal structure of KaiC^{te} (PDB ID: 4O0M). (**B**) Qualitative structural model of the interaction of CI^{te}* and fsKaiB (G89A,D91R-KaiB^{te}*) based on HDX-MS data and mutagenesis. Dark blue and cyan spheres represent CI residues whose mutations strongly or moderately weaken binding, respectively. Dark blue and cyan ribbons represent protection against H/D exchange upon complex formation that are >1.5 and 0.5 to 1.5 standard deviations above the average, respectively, as determined by HDX-MS (figs. S32 to S35).

Corrected 28 July 2015; see full text.

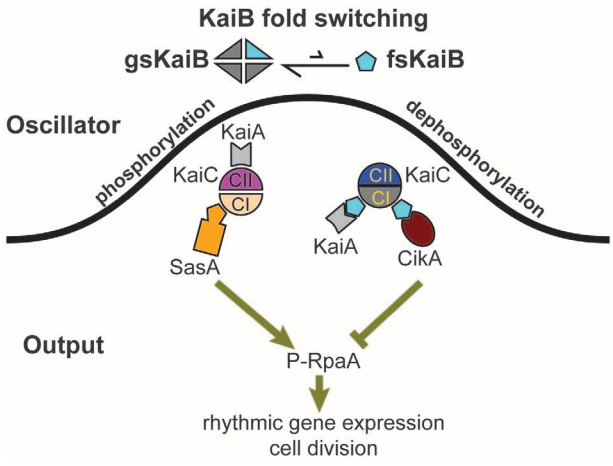

Fig. 5. Model of KaiB fold switching as linchpin for the cyanobacterial clock. Excursion of KaiB to the rare fold-switch state causes fsKaiB to displace SasA for binding to KaiC. KaiC-stabilized fsKaiB captures KaiA, initiating the dephosphorylation phase of the cycle. These aspects control oscillator period. CikA and KaiA compete for binding to fsKaiB, which further links oscillator function related to KaiA and output activity via CikA-mediated dephosphorylation of RpaA. The competitive interactions of fsKaiB with SasA, and KaiA with CikA, implicate "output components" CikA and SasA as parts of an extended oscillator.

this notion, a homolog of KaiB from *Legionella pneumophila*, with no known circadian rhythms, has an alanyl residue at position 89 and crystallizes in the fsKaiB fold (*31*) (fig. S41B). Rare excursions of KaiB between two distinct folds are essential for a robust circadian period and reciprocally regulate mutually antagonistic clock output–signaling pathways (Fig. 5).

REFERENCES AND NOTES

1. J. C. Dunlap, *Cell* **96**, 271–290 (1999).
2. M. Nakajima *et al.*, *Science* **308**, 414–415 (2005).
3. M. Ishiura *et al.*, *Science* **281**, 1519–1523 (1998).
4. T. Nishiwaki *et al.*, *Proc. Natl. Acad. Sci. U.S.A.* **101**, 13927–13932 (2004).
5. Single-letter abbreviations for the amino acid residues are as follows: A, Ala; C, Cys; D, Asp; E, Glu; F, Phe; G, Gly; H, His; I, Ile; K, Lys; L, Leu; M, Met; N, Asn; P, Pro; Q, Gln; R, Arg; S, Ser; T, Thr; V, Val; W, Trp; and Y, Tyr.
6. S. B. Williams, I. Vakonakis, S. S. Golden, A. C. LiWang, *Proc. Natl. Acad. Sci. U.S.A.* **99**, 15357–15362 (2002).
7. Y. Kitayama, H. Iwasaki, T. Nishiwaki, T. Kondo, *EMBO J.* **22**, 2127–2134 (2003).
8. Y. Xu, T. Mori, C. H. Johnson, *EMBO J.* **22**, 2117–2126 (2003).
9. H. Iwasaki *et al.*, *Cell* **101**, 223–233 (2000).
10. O. Schmitz, M. Katayama, S. B. Williams, T. Kondo, S. S. Golden, *Science* **289**, 765–768 (2000).
11. J. S. Markson, J. R. Piechura, A. M. Puszynska, E. K. O'Shea, *Cell* **155**, 1396–1408 (2013).
12. Y. G. Chang, R. Tseng, N. W. Kuo, A. LiWang, *Proc. Natl. Acad. Sci. U.S.A.* **109**, 16847–16851 (2012).
13. R. G. Garces, N. Wu, W. Gillon, E. F. Pai, *EMBO J.* **23**, 1688–1698 (2004).
14. S. A. Villarreal *et al.*, *J. Mol. Biol.* **425**, 3311–3324 (2013).
15. L. Holm, P. Rosenström, *Nucleic Acids Res.* **38** (Web Server), W545-W549 (2010).
16. I. Vakonakis *et al.*, *Proc. Natl. Acad. Sci. U.S.A.* **101**, 1479–1484 (2004).
17. G. Dong, Y. I. Kim, S. S. Golden, *Curr. Opin. Genet. Dev.* **20**, 619–625 (2010).
18. Y. Shen, F. Delaglio, G. Cornilescu, A. Bax, *J. Biomol. NMR* **44**, 213–223 (2009).
19. J. L. Martin, *Structure* **3**, 245–250 (1995).
20. A. G. Murzin, *Science* **320**, 1725–1726 (2008).
21. S. Raman *et al.*, *Science* **327**, 1014–1018 (2010).
22. I. Vakonakis, D. A. Klewer, S. B. Williams, S. S. Golden, A. C. LiWang, *J. Mol. Biol.* **342**, 9–17 (2004).
23. G. Dong *et al.*, *Cell* **140**, 529–539 (2010).
24. R. M. Smith, S. B. Williams, *Proc. Natl. Acad. Sci. U.S.A.* **103**, 8564–8569 (2006).
25. R. Tseng *et al.*, *J. Mol. Biol.* **426**, 389–402 (2014).
26. A. Gutu, E. K. O'Shea, *Mol. Cell* **50**, 288–294 (2013).
27. X. Zhang, G. Dong, S. S. Golden, *Mol. Microbiol.* **60**, 658–668 (2006).
28. T. Gao, X. Zhang, N. B. Ivleva, S. S. Golden, A. LiWang, *Protein Sci.* **16**, 465–475 (2007).
29. C. Phong, J. S. Markson, C. M. Wilhoite, M. J. Rust, *Proc. Natl. Acad. Sci. U.S.A.* **110**, 1124–1129 (2013).
30. J. Snijder *et al.*, *Proc. Natl. Acad. Sci. U.S.A.* **111**, 1379–1384 (2014).
31. M. Loza-Correa *et al.*, *Environ. Microbiol.* **16**, 359–381 (2014).
32. S. J. de Vries, M. van Dijk, A. M. J. J. Bonvin, *Nat. Protoc.* **5**, 883–897 (2010).

ACKNOWLEDGMENTS

We thank R. Greenspan, J.-P. Changeux, M. Paddock, Y. Shen, R. Peterson, S. Chou, and N.-W. Kuo for discussions and A. Chavan for figure preparation. Work was supported by Air Force Office of Scientific Research grant 13RSL012, Army Research Office grant W911NF1410056, and NIH grant GM107521 to A.L., a Burroughs-Wellcome Career Award at the Scientific Interface to M.J.R., NIH grants GM100116 and GM062419 to S.S.G. and AI081982 and AI101436 for support of the University of California–San Diego HDX-MS Laboratory, American Cancer Society Postdoctoral Fellowship PF-12-262-01-MPC to S.E.C., and NSF Graduate Research Fellowship to R.T. The data reported in this paper are tabulated in the supplementary materials.

SUPPLEMENTARY MATERIALS

www.sciencemag.org/content/349/6245/324/suppl/DC1
Materials and Methods
Figs. S1 to S41
Tables S1 to S14
References (*33*–*62*)

15 August 2014; accepted 8 May 2015
Published online 25 June 2015;
10.1126/science.1260031

SEX DETERMINATION

foxl3 is a germ cell–intrinsic factor involved in sperm-egg fate decision in medaka

Toshiya Nishimura,[1,2] Tetsuya Sato,[3,4] Yasuhiro Yamamoto,[1] Ikuko Watakabe,[1] Yasuyuki Ohkawa,[5] Mikita Suyama,[3,4] Satoru Kobayashi,[2,6]* Minoru Tanaka[1,2]†

Sex determination is an essential step in the commitment of a germ cell to a sperm or egg. However, the intrinsic factors that determine the sexual fate of vertebrate germ cells are unknown. Here, we show that *foxl3*, which is expressed in germ cells but not somatic cells in the gonad, is involved in sperm-egg fate decision in medaka fish. Adult XX medaka with disrupted *foxl3* developed functional sperm in the expanded germinal epithelium of a histologically functional ovary. In chimeric medaka, mutant germ cells initiated spermatogenesis in female wild-type gonad. These results indicate that a germ cell–intrinsic cue for the sperm-egg fate decision is present in medaka and that spermatogenesis can proceed in a female gonadal environment.

In vertebrates, gonadal somatic cells instruct germ cells to adopt their sexual fates. In medaka (*Oryzias latipes*), the expression of *DMY*/*dmrt1bY* in the supporting somatic cells is critical for the fate decision of germ cells to enter spermatogenesis (*1*, *2*). However, the molecular mechanism underlying the sexual fate decision in germ cells remains unknown. In this study, we show that *foxl3* serves as a germ cell–intrinsic cue for sperm-egg fate decision.

foxl3 is an ancient duplicated copy of *foxl2* that is expressed in gonads of teleost fish (*3*–*5*). Although *foxl2* is known to be essential for ovarian development and maintenance (*6*–*9*), the function of *foxl3* is not known. *foxl3* transcripts and FOXL3 protein (*foxl3*/FOXL3) were first detectable in germ cells of both XX and XY embryos at stage 35, the time of onset of gonadal sex differentiation (figs. S1, A to D, and S2, A to D). After this stage in XX

[1]Laboratory of Molecular Genetics for Reproduction, National Institute for Basic Biology, Okazaki 444-8787, Japan. [2]Graduate University for Advanced Studies (SOKENDAI), Okazaki 444-8585, Japan. [3]Medical Institute of Bioregulation, Kyushu University, Fukuoka 812-8582, Japan. [4]Core Research for Evolutional Science and Technology (CREST), Japan Science and Technology Agency (JST), Fukuoka 812-8582, Japan. [5]Department of Advanced Medical Initiatives, JST-CREST, Faculty of Medicine, Kyushu University, Fukuoka 812-8582, Japan. [6]Okazaki Institute for Integrative Bioscience, National Institute for Basic Biology, Okazaki 444-8787, Japan.
*Present address: Life Science Center of Tsukuba Advanced Research Alliance, University of Tsukuba, Tsukuba, Ibaraki 305-8577, Japan. †Corresponding author. E-mail: mtanaka@nibb.ac.jp

Science
AAAS

A protein fold switch joins the circadian oscillator to clock output in cyanobacteria

Yong-Gang Chang *et al.*

Science **349**, 324 (2015);
DOI: 10.1126/science.1260031

Science (print ISSN 0036-8075; online ISSN 1095-9203) is published weekly, except the last week in December, by the American Association for the Advancement of Science, 1200 New York Avenue NW, Washington, DC 20005.